Science Advances
AAAS

advances.sciencemag.org/cgi/content/full/3/3/e1601284/DC1

Supplementary Materials for

Radar interferometry offers new insights into threats to the Angkor site

Fulong Chen, Huadong Guo, Peifeng Ma, Hui Lin, Cheng Wang, Natarajan Ishwaran, Peou Hang

Published 3 March 2017, *Sci. Adv.* **3**, e1601284 (2017)
DOI: 10.1126/sciadv.1601284

This PDF file includes:

SUPPLEMENTARY MATERIALS

Materials and Methods

45 scenes of synthetic aperture radar (SAR) images of German twin Earth-observation satellites TerraSAR/TanDEM-X were used for the interferometric analysis. Single look complex (SLC) X-band (3.1 cm wavelength) SAR data were acquired for the period from Feb. 16, 2011 to Dec. 16, 2013 in the Stripmap mode and a nominal radar look angle of 44° along the ascending orbit. The temperature data corresponding to SAR acquisitions were collected for modeling thermal amplitudes of materials. Taking the acquisition of Nov. 4, 2012 as the reference image to minimize the spatio-temporal de-correlation, parameters of the interferogram formation, the temperature data for Tomo-PSInSAR are summarized in table S1.

The motion component can be quantitatively validated by the height component considering the concurrence of high-accurate inversion of these two unknown parameters using the Tomo-PSInSAR models, particularly for the case of unavailable motion data on site. In this study, estimated heights on 50 PSs of the terrace gallery were quantitatively compared with ground-based measurements during the field visits undertaken in 2014 (fig. S5), resulting in a standard deviation σ_h = 0.44 m that is equivalent to a phase error σ_ϕ = 0.47 rad using Equation $\sigma_\phi \cong \frac{4\pi\sigma_{B_n}\sigma_h\sqrt{M}}{\lambda R\sin\theta}$ and then equivalent to an internal motion precision of 0.2 mm/yr based on using another Equation $\sigma_v \cong \frac{\lambda\sigma_\phi}{4\pi\sigma_{Bt}\sqrt{M}}$; where σ_{B_n} = 196 m and σ_{B_t} = 0.81 yr are the normal- and temporal-baseline standard dispersions, respectively. M = 45 is the number of SAR images acquired, λ = 0.031 m is the radar wavelength, θ = 44°is the looking angle, and R = 715 km is the sensor-target distance. InSAR results reported could also be validated by the calculated linear thermal expansion coefficient of temple materials, such as 5.0–6.0×10^{-5} for sandstones.

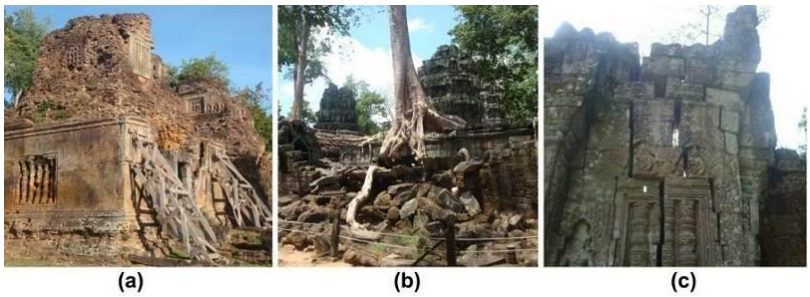

fig. S1. Collapsing monuments in Angkor site. Collapse events could be caused by (**a**) decay, (**b**) tree growth and (**c**) defects in the soil subsurface and the foundation of the monument. Photographs were provided by Fulong Chen from Institute of Remote Sensing and Digital Earth, Chinese Academy of Sciences.

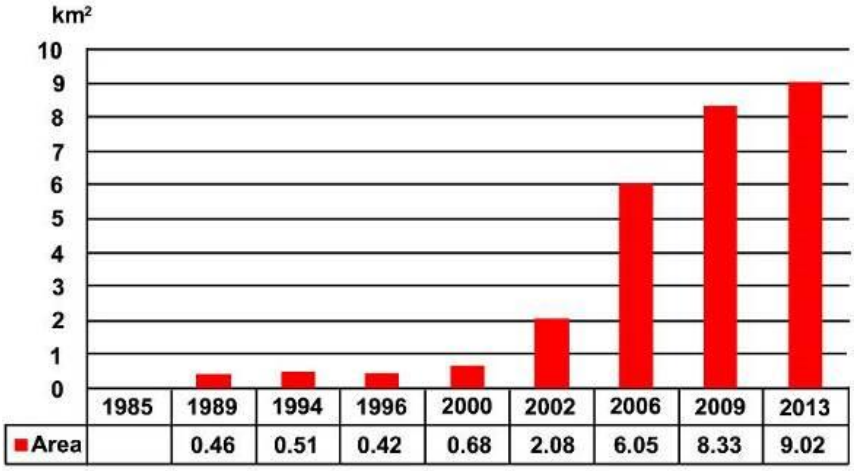

fig. S2. Extension of urban land use estimated by the comparison of multitemporal Landsat images for the period 1985–2013. In the years after 2000 urban land-cover increased sharply and was beginning to plateau during 2011–2013.

fig. S3. Field photos of wells for pumping groundwater. Photographs of public **(a)** and private **(b)** wells were provided by Fulong Chen from Institute of Remote Sensing and Digital Earth, Chinese Academy of Sciences.

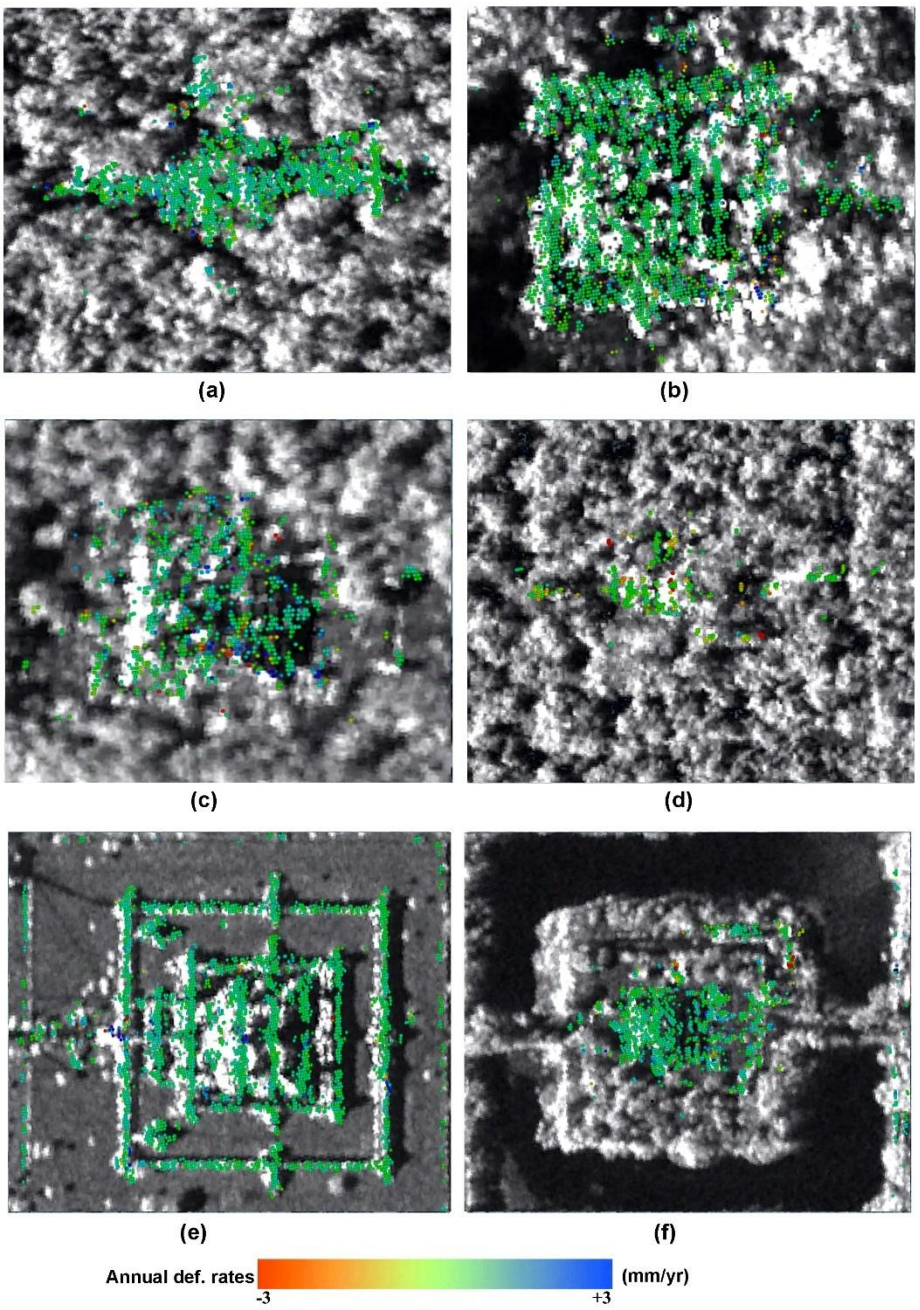

fig. S4. Monument-scale Tomo-PSInSAR derived annual deformation rates in ancient temples (overlaid on the averaged amplitude of SAR imagery). Spatial motion heterogeneities on (**a**) Preah Khan, (**b**) Bayon, (**c**) Ph.Bakheng, (**d**) Ta Prohm, (**e**) Angkor Wat and (**f**) Bakong are evident due to the enhanced PS targets extracted. TerraSAR/TanDEM-X data were provided by Deutschen Zentrums für Luft- und Raumfahrt (DLR, http://sss.terrasar-x.dlr.de/) under the General AO project (CAL2073).

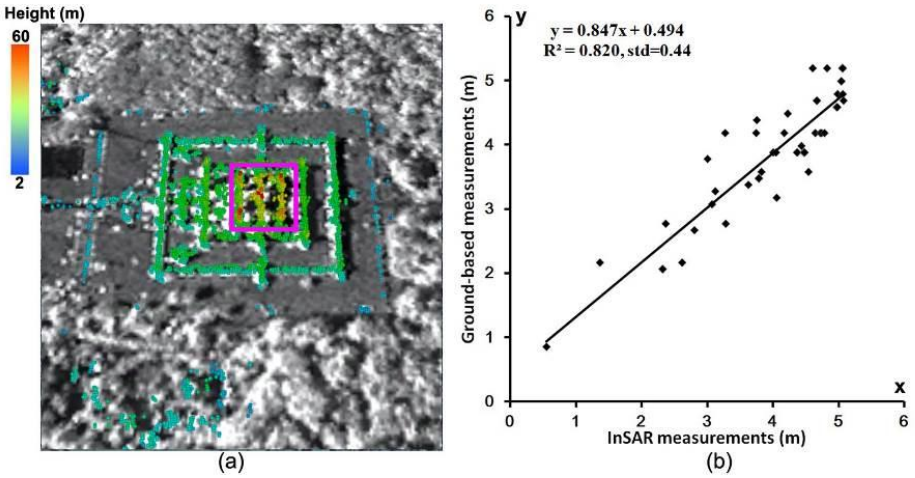

fig. S5. Validation of Tomo-PSInSAR–derived motions using the PS heights confirmed by field investigations undertaken in 2014. (**a**) Precise height estimation of Angkor Wat monument with temple-mountain shapes (overlaid on the averaged amplitude of SAR imagery), marked by the pink rectangle; (**b**) Scatter-plot of estimated heights compared with the ground-truth on the terrace gallery, indicating a consistent trend supported by a significant correlation coefficient of 0.820 with a standard deviation of 0.44 m. TerraSAR/TanDEM-X data were provided by Deutschen Zentrums für Luft- und Raumfahrt (DLR, http://sss.terrasar-x.dlr.de/) under the General AO project (CAL2073).

table S1. Parameters of acquisition and interferogram formation of TerraSAR/TanDEM-X SAR images and the corresponding temperature data (10 a.m. local time) used in this study; the acquisition of 4 November 2012 (marked by the star) was selected as the reference image.

Acquisitions (yyyymmdd)	Normal baseline (m)	Temporal baseline (yr)	Temperature (°C)
20110216	-41.5956	-1.71781	31
20110310	248.3855	-1.65753	29
20110321	-292.4068	-1.6274	33
20110401	-55.8115	-1.59726	33
20110412	291.4081	-1.56712	31
20110504	231.9028	-1.50685	34
20110526	-0.6569	-1.44658	27
20110617	-125.7945	-1.3863	32
20110709	-238.6831	-1.32603	33
20110720	-153.8763	-1.29589	31
20111016	-174.9263	-1.05479	25
20120225	-93.0024	-0.69315	34
20120307	-47.0729	-0.66301	33
20120318	-47.3900	-0.63288	30
20120409	-18.1904	-0.5726	32
20120420	414.2893	-0.54247	34
20120512	-139.1623	-0.48219	33
20120603	-102.9868	-0.42192	32
20120614	-92.4931	-0.39178	32
20120706	353.6982	-0.33151	29
20120717	474.8715	-0.30137	33
20120819	149.3447	-0.21096	32
20120830	398.0299	-0.18082	26
20120921	-122.4522	-0.12055	27
20121002	-136.1018	-0.09041	32
20121024	-221.0997	-0.03014	30
20121104*	0	0	32
20121207	-244.7639	0.090411	29
20121229	17.9455	0.150685	30
20130109	-179.0715	0.180822	30
20130120	224.6224	0.210959	28
20130131	-156.0594	0.241096	29
20130211	100.0474	0.271233	28
20130305	-40.2014	0.331507	30
20130316	27.0516	0.361644	32
20130418	-260.9224	0.452055	32
20130429	-181.5392	0.482192	33
20130510	-21.6628	0.512329	33
20130521	208.9209	0.542466	33
20130612	192.0488	0.60274	27
20130623	228.0042	0.632877	30
20130704	14.5760	0.663014	28
20130908	-128.9617	0.843836	31
20131113	-94.5858	1.024658	33
20131216	-47.9337	1.115069	29
Standard dispersions of normal- and temporal-baselines	196.3551	0.809651	Average temperature=30.8